Rojava Journal of Science and Technology

2026, VOL. 3, No 1, [102-120]

Hierarchical Fe_3O_4@Mg/Al-LDH@Chitosan Nanocomposite for Rapid and Reusable Congo Red Adsorption from Complex Water Systems

Jwan Sheikh Mohammad[1], Haidar Saify Nabiabad2, Mohamed E.Mahmoud[3], Rehab M .El-Sharkawy*[4]

[1]Dep. of Analytical Chemistry, Institute of Science and Modern Technology -Rojava University, Syria.

[2]Dep. of Biotechnology, Institute of Science and Modern Technology -Rojava University, Syria.

[3]Faculty of Science, Chemistry Department, Alexandria University, Egypt

[4]Faculty of Dentistry, Chemistry Department, Pharos University in Alexandria, Egyp

ABSTRACT

Synthetic dye contamination represents a persistent challenge in wastewater management due to the chemical stability and toxicity of these compounds. This study presents the synthesis and evaluation of a magnetically recoverable nanocomposite composed of magnetite, layered double hydroxide (LDH), and chitosan (Fe_3O_4@LDH@CS) for the removal of Congo Red from aqueous systems. The material was prepared using a microwave-assisted approach designed to enhance synthesis efficiency and reduce energy consumption. Comprehensive characterization (XRD, FTIR, SEM, and TGA) confirmed the successful integration of magnetite nanoparticles within an LDH matrix stabilized by chitosan, resulting in a structurally robust and porous hybrid adsorbent. Batch adsorption experiments demonstrated high removal efficiencies (>95%) across a broad pH range, with optimal performance near neutral conditions. Kinetic analysis indicated that adsorption followed a pseudo-second-order model, suggesting chemisorption as the dominant mechanism, while isotherm modeling supported monolayer adsorption behavior. Thermodynamic parameters revealed that the process is spontaneous and endothermic, with improved adsorption at elevated temperatures. The nanocomposite maintained high performance over multiple regeneration cycles and showed strong applicability in real water matrices, including industrial wastewater and seawater. These findings highlight the potential of Fe_3O_4@LDH@CS as an efficient and reusable adsorbent for practical dye remediation applications.

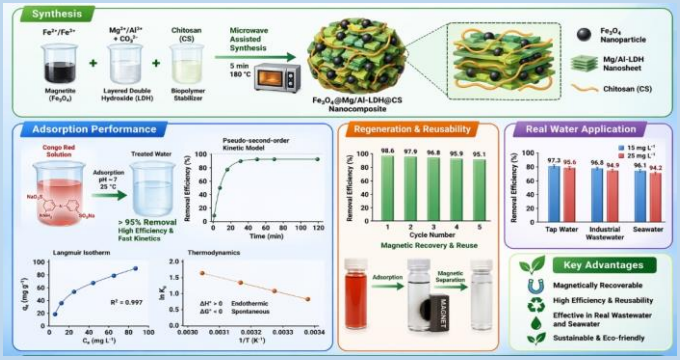

ARTICLE HISTORY

Received: 14 Jan. 2026

Revised: 10 Jul. 2026

Accepted: 18 Sep. 2026

Keywords: Magnetite-layered double hydroxide, Chitosan, nanocomposite, Congo red dye, wastewater treatment

*Corresponding Author: rehab.mansour@pu

1. Introduction

The discharge of dye-containing effluents into aquatic environments remains a significant environmental concern, particularly in regions with intensive textile, printing, and chemical manufacturing activities. Synthetic dyes are designed to resist fading and degradation, resulting in high persistence once released into natural water systems (Lin et al., 2023). Their presence not only affects water aesthetics but also reduces light penetration, disrupts aquatic ecosystems, and introduces toxic, mutagenic, and potentially carcinogenic compounds into the environment (Oguanobi et al., 2025). Among commonly used dyes, Congo Red is a widely applied anionic azo dye known for its high solubility and structural stability. These properties make it particularly difficult to remove through conventional treatment methods (Khan et al., 2022). Once introduced into water bodies, Congo Red can degrade into aromatic amines, which pose additional environmental and health risks. As a result, the development of efficient and sustainable technologies for dye removal is a critical priority in environmental remediation. Traditional treatment approaches, including biological degradation, coagulation–flocculation, and advanced oxidation processes, have demonstrated varying degrees of effectiveness. However, these methods are often limited by high operational costs, incomplete removal, or the generation of secondary pollutants (Zazouli et al., 2024). Adsorption has emerged as a preferred alternative due to its operational simplicity, high efficiency, and adaptability to different wastewater compositions. The effectiveness of adsorption processes depends largely on the properties of the adsorbent, including surface area, functional groups, and structural stability (Younas et al., 2021). Recent advances in nanotechnology have enabled the design of novel adsorbent materials with enhanced performance characteristics. Magnetite (Fe_3O_4) nanoparticles have received considerable attention due to their high surface reactivity and the advantage of magnetic separation, which simplifies post-treatment recovery. Despite these benefits, magnetite nanoparticles tend to aggregate and oxidize, reducing their long-term stability and adsorption efficiency (Arrisujaya et al., 2025). Layered double hydroxides (LDHs) offer complementary properties that address some of these limitations. LDHs are characterized by positively charged layers and exchangeable interlayer anions, enabling strong interactions with negatively charged contaminants such as azo dyes (Zhang et al., 2026). Their tunable composition and relatively high thermal stability make them attractive candidates for environmental applications. However, LDHs alone often suffer from poor mechanical strength and limited reusability under repeated operational cycles (Wang et al., 2026). Chitosan, a naturally derived biopolymer, has also been extensively studied for pollutant removal due to its abundance, biodegradability, and functional amino and hydroxyl groups. These functional groups provide active binding sites for dye molecules through electrostatic interactions and hydrogen bonding (Cui et al., 2026). Nevertheless, the practical application of chitosan is constrained by its limited mechanical stability and solubility under acidic conditions (Tundwal et al., 2026). To overcome the individual limitations of these materials, recent research has focused on the development of hybrid nanocomposites that combine their complementary properties. Integrating magnetite, LDH, and chitosan into a single composite structure offers several advantages: enhanced adsorption capacity, improved structural stability, and convenient magnetic recovery. Such multifunctional materials are particularly attractive for real-world remediation applications, where operational efficiency and reusability are critical. In this study, a Fe_3O_4@LDH@Chitosan nanocomposite was synthesized using a microwave-assisted method, which provides a rapid and energy-efficient alternative to conventional synthesis techniques. The performance of

the synthesized material was evaluated for the removal of Congo Red from aqueous solutions under varying experimental conditions, including pH, contact time, temperature, and adsorbent dosage. In addition to controlled laboratory experiments, the applicability of the nanocomposite was assessed using real water samples to better reflect environmental conditions. The objective of this work is to demonstrate the effectiveness of this hybrid material as a practical adsorbent for dye-contaminated wastewater and to provide insights into the mechanisms governing the adsorption process. By combining material innovation with application-oriented evaluation, this study contributes to the development of sustainable and efficient solutions for water pollution remediation.

2. Materials and Methods

All chemicals used in this study were of analytical grade and used without further purification to ensure reproducibility. Magnesium chloride hexahydrate ($MgCl_2 \cdot 6H_2O$), aluminum chloride hexahydrate ($AlCl_3 \cdot 6H_2O$), sodium hydroxide (NaOH), sodium carbonate (Na_2CO_3), hydrochloric acid (HCl), and Congo Red dye were obtained from Sigma. Chitosan (degree of deacetylation ≈ 85–90%) was used as the biopolymeric component. Deionized water was employed in all synthesis and adsorption experiments to minimize interference from dissolved ions. Magnetite (Fe_3O_4) nanoparticles were synthesized in laboratory using a co-precipitation method to ensure control over particle size and purity.

2.1. Microwave-Assisted Synthesis of Nanomagnetite (nFe_3O_4)

Magnetite nanoparticles were synthesized via a modified co-precipitation approach under microwave-assisted conditions to enhance reaction kinetics and particle homogeneity. Briefly, ferrous (Fe^{2+}) and ferric (Fe^{3+}) salts were dissolved in an acidic aqueous medium under continuous stirring. The molar ratio of Fe^{2+} to Fe^{3+} was maintained at 1:2 to favor magnetite formation (Mystrioti et al., 2022).

A sodium hydroxide solution was added dropwise under vigorous stirring to induce precipitation. The reaction mixture was intermittently exposed to microwave irradiation to maintain a temperature of approximately 80°C, accelerating nucleation and growth processes. The resulting black precipitate was magnetically separated, washed repeatedly with deionized water to remove residual ions, and dried at 70°C.

2.2. Preparation of Magnesium–Aluminum Layered Double Hydroxide (Mg/Al-LDH)

The Mg/Al-LDH was synthesized using a conventional co-precipitation method under controlled alkaline conditions. A mixed metal solution containing Mg^{2+} and Al^{3+} ions at a molar ratio of 3:1 was prepared and heated under continuous stirring.

A basic solution containing NaOH and Na_2CO_3 was added dropwise to the metal solution while maintaining the pH at approximately 10. The suspension was aged at elevated temperature (≈80°C) for 24 hours to promote crystallization and structural ordering of the LDH layers. The precipitate was then filtered, washed to neutral pH, and dried to obtain a fine powder.

2.3. Microwave-Assisted Synthesis of CT@Fe_3O_4@Mg/Al-LDH Nanocomposite

The hybrid nanocomposite was prepared through a sequential assembly process combining 5.0 g magnetite, LDH, and 5.0 g chitosan. Initially, Fe_3O_4 nanoparticles were mixed with chitosan in the presence of a small volume of water to ensure uniform dispersion. The mixture was subjected to microwave heating to facilitate partial dehydration and enhance interaction between the inorganic and polymeric phases.

Subsequently, the Fe_3O_4–chitosan composite was blended with 5.0 g Mg/Al-LDH and further treated under microwave irradiation. This process was repeated multiple times to ensure homogeneous integration of all components. The final product was ground, sieved, and dried to obtain a stable, magnetically responsive CT@Fe_3O_4@Mg/Al-LDH nanocomposite.

2.4. Nanocomposite Characterization

The structural and physicochemical characteristics of the nanocomposite were analyzed using various analytical methods. The surface morphology was investigated through scanning electron microscopy (SEM) employing a Hitachi S-4800 instrument. To enhance conductivity, the samples were coated with a thin layer of Au–Pd. X-ray diffraction (XRD) analysis was carried out to determine the crystalline phases and structural features. Fourier-transform infrared spectroscopy (FTIR) was utilized to detect functional groups within the range of 4000–500 cm^{-1} using KBr pellet techniques. Additionally, thermogravimetric analysis (TGA) was performed in a nitrogen atmosphere from 25 to 800 °C at a heating rate of 10 °C min^{-1} to assess thermal stability.

2.5. Microwave-Enhanced Removal of Congo Red (CR) Dye

A stock solution of Congo Red (CR) dye with a concentration of 1000 ppm will be used as the primary source solution. From this stock, working solutions with concentrations of 5, 10, and 15 mg/L will be prepared by appropriate dilution using double-distilled water (DW). The absorbance of CR dye will be measured at its maximum wavelength (λ_{max} = 497 nm) using a UV–Vis spectrophotometer. Microwave-assisted adsorption and decolorization experiments will be conducted using the synthesized Fe_3O_4@Chitosan@Mg/Al-LDH nanocomposite under varying operational conditions, including different nanocomposite doses, contact times, initial dye concentrations, pH values, temperatures, and coexisting ions. The dye removal efficiency (%E) of Congo Red onto the nanocomposite will be determined using Equation (1):

$$\%E = (C_0 - C)/C_0$$

where C_o and C_e represent the initial and equilibrium concentrations (mg/L) of CR, respectively.

2.6. Adsorption Experiments

Batch adsorption experiments were carried out to assess the removal efficiency of Congo Red under microwave-assisted conditions. A stock solution of the dye was initially prepared and subsequently diluted to the required concentrations for experimental analysis. The adsorption studies were performed in conical flasks containing a fixed volume of dye solution and a predetermined mass of adsorbent. The mixtures were exposed to microwave irradiation in order to enhance mass transfer and improve adsorption kinetics. The effects of key operational parameters, including initial solution pH, adsorbent dosage, contact time, initial dye concentration, and temperature, were systematically investigated. The solution pH was adjusted using dilute hydrochloric acid (HCl) or sodium hydroxide (NaOH) solutions. Following treatment, the adsorbent was separated magnetically, and the residual dye concentration in the solution was determined using a UV–Vis spectrophotometer at a wavelength of 497 nm. The removal efficiency (%) and adsorption capacity were calculated based on standard mass balance equations. All experiments were

performed in triplicate to ensure reproducibility and reliability of the obtained data.

2.7. Kinetic and Isotherm Modeling

To elucidate the adsorption mechanism, the experimental data were analyzed using a series of kinetic and equilibrium isotherm models. Kinetic analyses were performed employing the pseudo-first-order, pseudo-second-order, intraparticle diffusion, Elovich, and Avrami models in order to identify the rate-controlling steps governing the adsorption process. Equilibrium data were interpreted using the Langmuir, Freundlich, Temkin, and Dubinin–Radushkevich isotherm models to characterize adsorption behavior and surface properties of the adsorbent. The model parameters were determined via linear regression, and the goodness of fit was evaluated based on the corresponding correlation coefficients (R^2).

2.8. Thermodynamic Analysis

Thermodynamic parameters, including Gibbs free energy (ΔG°), enthalpy (ΔH°), and entropy (ΔS°), were determined from temperature-dependent adsorption experiments. The Van't Hoff equation was used to analyze the relationship between temperature and adsorption equilibrium. These parameters provided insight into the spontaneity, feasibility, and nature of the adsorption process.

2.9. Application to Real Water Samples

To evaluate practical applicability, the synthesized nanocomposite was tested using real water samples, including tap water, industrial wastewater, and seawater. These samples were spiked with Congo Red and treated under optimized conditions. The performance of the adsorbent in complex matrices was assessed by comparing removal efficiencies with those obtained in controlled laboratory conditions.

3. Results and discussion

3.1. Structural and Physicochemical Characteristics

The XRD analysis confirmed the successful formation of a hybrid nanocomposite consisting of magnetite and LDH phases. The presence of characteristic diffraction peaks corresponding to magnetite indicates that the crystalline structure was preserved during composite fabrication. Meanwhile, the broadened LDH peaks suggest partial structural disorder, likely due to interaction with chitosan and magnetite nanoparticles.

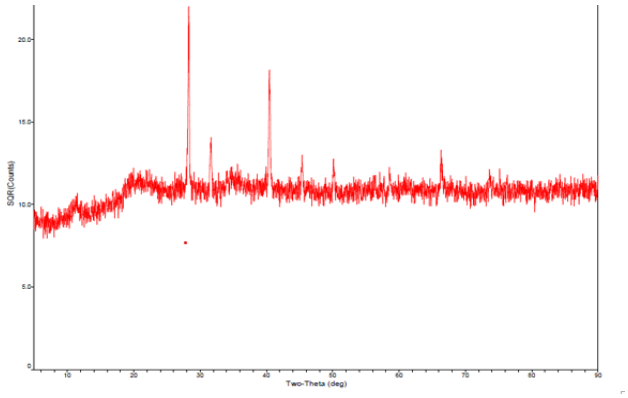

Figure 1: X-ray diffraction (XRD) patterns of Fe_3O_4, Mg/Al-LDH, and Fe_3O_4@Mg/Al-LDH@CS nanocomposite, confirming the successful incorporation of magnetite into the LDH matrix without structural collapse of the crystalline phases.

FTIR spectra further supported the successful integration of all components. The coexistence of Fe–O vibrations and hydroxyl-related bands indicate strong interactions between magnetite, LDH layers, and chitosan functional groups. The observed band broadening suggests hydrogen bonding and interfacial coupling, which are beneficial for adsorption processes.

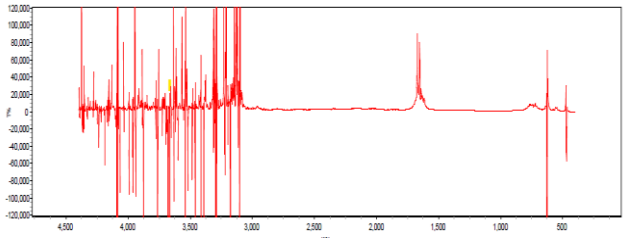

Figure 2: Fourier-transform infrared (FTIR) spectra of Fe_3O_4@Mg/Al-LDH@CS nanocomposite, showing characteristic bands of Fe–O, hydroxyl groups, and chitosan functional groups, indicating strong interfacial interactions among composite components.

Thermogravimetric analysis revealed multiple weight-loss stages corresponding to moisture removal, decomposition of organic components, and structural transformations. The relatively high residual mass confirms the presence of thermally stable inorganic phases, indicating that the composite can withstand elevated temperatures encountered in practical applications (Kan et al., 2025).

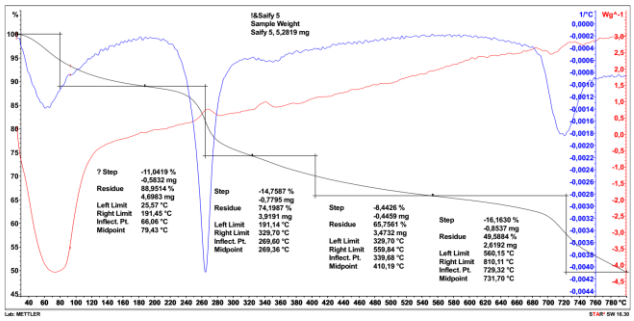

Figure 3: Thermogravimetric analysis (TGA) curve of Fe_3O_4@Mg/Al-LDH@CS nanocomposite, illustrating multi-step weight loss associated with moisture removal, chitosan decomposition, and structural stability of inorganic phases.

Figure 4 presents the SEM micrograph of the synthesized magnetite-loaded layered double hydroxide (LDH) composite incorporated with chitosan. The observed morphology is predominantly composed of irregular, fractured, plate-like particles, which is typical of LDH-based materials combined with partially aggregated magnetite domains. The composite exhibits heterogeneous and non-uniform particle sizes, ranging from tens to several hundreds of nanometers. The irregular shapes and sharp edges indicate the coexistence of crystalline LDH layers and fragmented magnetite clusters, reflecting the brittle nature of the material following synthesis and mechanical processing. The particle surfaces appear rough, cracked, and highly textured. This surface morphology suggests the presence of layered LDH structures alongside embedded or partially coated magnetite nanoparticles. Although a continuous chitosan film is not clearly visible at this magnification, it is likely present as a binding agent within the composite matrix. Such surface roughness is advantageous for adsorption processes, as it increases the availability of active sites for Congo Red dye uptake (Xiao et al., 2026). Moderate agglomeration of particles is evident, which can be attributed to electrostatic interactions between LDH layers, magnetic interactions among Fe_3O_4 domains, and hydrogen bonding associated with chitosan functional groups. This aggregation behavior contributes to the structural stability of the hybrid composite. Additionally, the micrograph reveals the presence of interparticle voids with varying sizes. These voids may facilitate mass transfer during adsorption by providing accessible pathways for dye molecules. However, due to the relatively low magnification, nanoscale porosity cannot be accurately assessed.

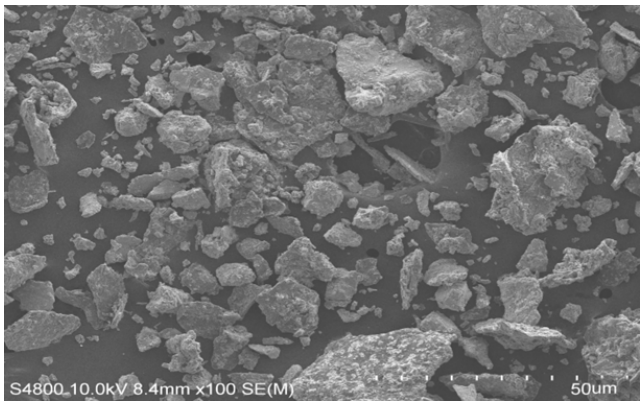

Figure 4: Scanning electron microscopy (SEM) image of Fe_3O_4@Mg/Al-LDH@CS nanocomposite, revealing irregular, plate-like morphology with rough and porous surface features favorable for adsorption.

3.2. Effect of pH and Surface Charge Behavior

Solution pH plays a critical role in adsorption processes by influencing both the surface charge of the adsorbent

and the ionization state of the dye. The nanocomposite exhibited high removal efficiency across a wide pH range, with optimal performance observed near neutral conditions. The point of zero charge (pHpzc ≈ 5) indicates that the surface is positively charged at acidic pH values, promoting electrostatic attraction with anionic Congo Red molecules. At higher pH values, despite reduced electrostatic attraction, adsorption efficiency remained high, suggesting the involvement of additional mechanisms such as hydrogen bonding and π–π interactions. This broad pH tolerance is particularly important for real-world applications, where wastewater pH can vary significantly. The combined evaluation of adsorption efficiency and pHpzc confirms that the Magnetite–LDH–Chitosan nanocomposite exhibits strong affinity toward Congo Red across a broad pH range, with optimum performance around pH 5–7 and a pHpzc close to 5.0, supporting a mechanism governed by electrostatic interactions, hydrogen bonding, and partial surface complexation (Chaimaa et al., 2026).

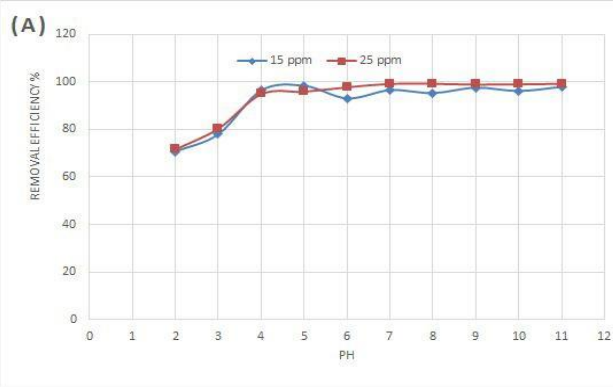

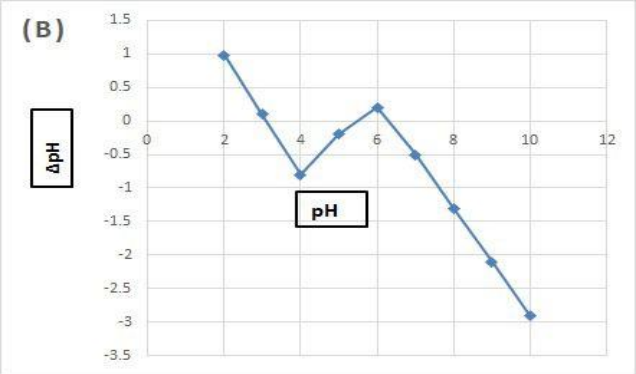

Figure 5: (A) Effect of initial solution pH on Congo Red removal efficiency using Fe_3O_4@Mg/Al-LDH@CS nanocomposite; (B) determination of point of zero charge (pHpzc ≈ 5) at 25 °C, indicating pH-dependent surface charge behavior.

3.3. Effect of Contact Time and Adsorption Kinetics

The kinetic model equations and corresponding parameters for Congo Red adsorption onto the Magnetite–LDH–Chitosan nanocomposite were evaluated (Table 1). Figure 6A shows the effect of contact time on removal efficiency at initial concentrations of 15 and 25 ppm. Adsorption proceeded rapidly at the initial stage, followed by a gradual approach to equilibrium. Within the first 10 min, removal efficiencies reached ~94–96% (15 ppm) and 97–98% (25 ppm), attributed to the abundance of available active sites. With increasing contact time, the removal efficiency increased slightly and attained equilibrium within 40–60 min, stabilizing at ~97–98% for 15 ppm and ~99% for 25 ppm. This behavior indicates rapid site occupation followed by saturation. The two-stage profile suggests that surface adsorption dominates initially, while intraparticle diffusion contributes at later stages, confirming the favorable kinetics of the nanocomposite. Figure 6 B presents the pseudo-first-order model. The plots of $\ln(q_e - q_t)$ versus t show limited linearity, indicating that this model is only applicable during the early adsorption stage. The deviation at longer contact times suggests that adsorption is not governed solely by physical interactions. In contrast, the pseudo-second-order model (Figure 6C) shows excellent linearity in plots of

t/q_t versus t, indicating a good fit to the experimental data. This suggests that chemisorption, involving electron sharing or exchange between dye molecules and surface functional groups, controls the adsorption process. The Avrami model (Figure 6D) also exhibits good linearity for both concentrations, indicating its suitability for describing the system. This reflects heterogeneous adsorption behavior involving multiple concurrent mechanisms. The slightly higher slope at 25 ppm suggests a faster approach to equilibrium, likely due to a higher driving force.

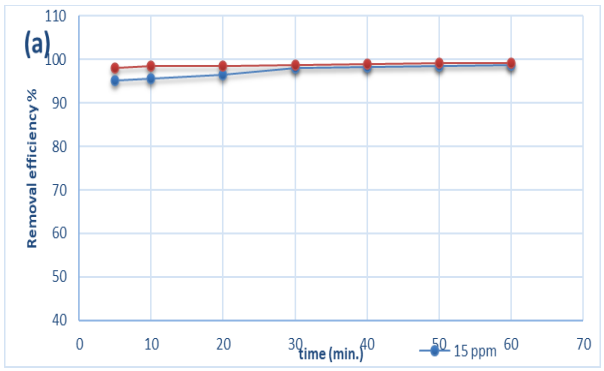

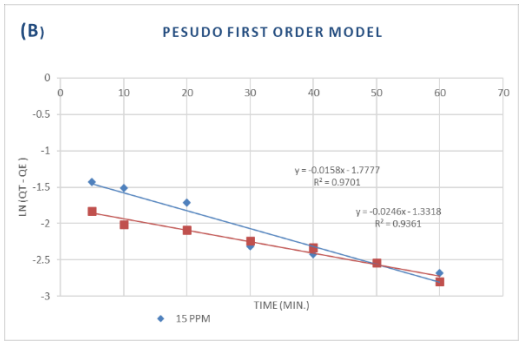

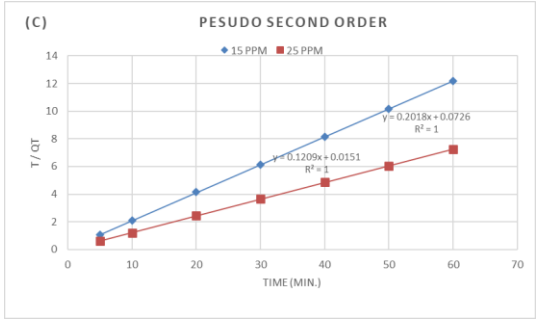

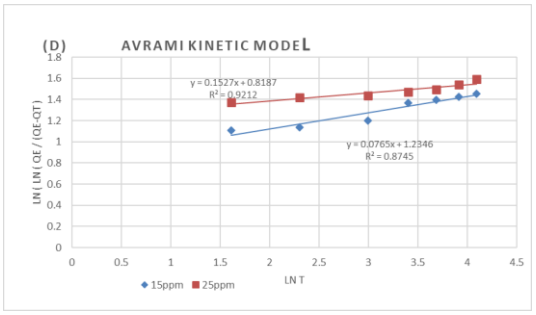

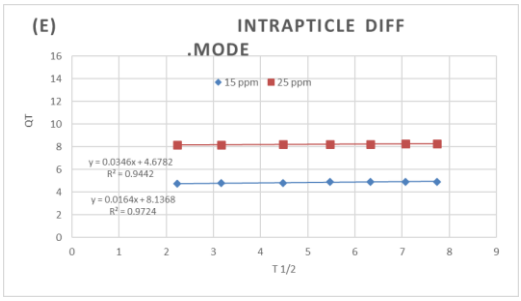

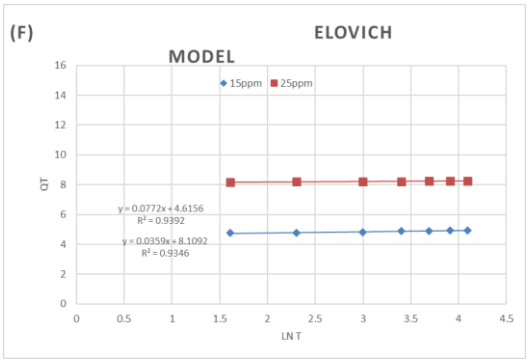

Figure 6: Adsorption kinetics of Congo Red onto Fe_3O_4@Mg/Al-LDH@CS nanocomposite at 25 °C: (A) effect of contact time; (B) pseudo-first-order model; (C) pseudo-second-order model; (D) Avrami model; (E) intraparticle diffusion model; (F) Elovich model, demonstrating chemisorption-dominated adsorption behavior.

Figure 6E presents the intraparticle diffusion plots based on the Weber–Morris model, obtained by plotting Q_tagainst t^(1/2)for Congo Red solutions at initial concentrations of 15 ppm and 25 ppm. In both cases, the plots deviate from the origin, indicating that intraparticle diffusion is not the sole rate-limiting step governing the adsorption process. The observed multilinear profiles suggest the occurrence of multiple sequential stages, initially dominated by boundary-layer diffusion, followed by a slower intraparticle diffusion phase within the porous structure of the adsorbent. Moreover, the higher intercept values observed for the 25 ppm system imply an increased contribution of surface diffusion at elevated dye concentrations, whereas the 15

ppm system exhibits comparatively lower diffusion resistance. These findings collectively demonstrate that, although intraparticle diffusion plays a significant role, it does not exclusively control the adsorption kinetics. Figure 6F depicts the adsorption kinetics analyzed using the Elovich model for Congo Red uptake onto the synthesized nanocomposite. The linear relationship between q_tand ln$f_0$tindicates a good fit to the Elovich equation, suggesting that the adsorption occurs on a heterogeneous surface. This behavior reflects a complex adsorption mechanism in which the adsorption rate progressively decreases with increasing surface coverage due to the gradual occupation of active sites (Jomardani et al., 2026). The applicability of the Elovich model further supports the presence of strong interactions between Congo Red molecules and the functional groups of the adsorbent, consistent with a chemisorption-dominated mechanism.

Table 1. Equations of kinetic models and their parameters for the adsorptive removal of Magnetite–LDH–Chitosan.

Kinetic Model	**Equation**	**Plot**	**Kinetic Parameter**	**RRD 15 ppm**	**RRD 25 ppm**
Pseudo-First Order	$Ln\,(q_e - q_t) = Ln\,(q_e) - k_1 t$	$ln\,(q_e - q_t)$ versus time (t), q_e and q_t are the sorption capacity at equilibrium and at time t (min), respectively, k_1 is the first order rate constant	q_e (mg/g) (calc)	4.997667	8.331
			K_1 (min^{-1})	0.0246	0.0158
			R^2	0.9361	0.9701
Pseudo-Second Order	$t/q_t = 1/k_2 q_e^2 + t/q_e$	t/q_t versus time (t), K_2 is the second order rate constant	q_e (mg/g) (exp)	4.92	8.2533333
			q_e (mg/g) (calc)	4.9554014	8.2712986
			K_2 (g/mg min)	0.102364036	0.382394
			R^2	1	1
Intra-particle Diffusion	$q_t = k_{id}\, t^{0.5} + C$	q_t versus ($t^{0.5}$), C is the thickness of the adsorption layer, K_{id} is the intra-particle order rate constant	K_{id} (mg/g $min^{0.5}$)	0.0346	0.0164
			C	4.6782	8.1368
			R^2	0.9442	0.9724
Elovich	$q_t = 1/\beta\, Ln(\alpha\beta) + 1/\beta\, Ln\,(t)$	q_t versus ln t, α is the initial adsorption rate, β is related to the extent of surface coverage and the activation energy for the chemisorption process	α (mg/g min)	7.129	4.517
			β (mg/g)	12.95337	27.85515
			R^2	0.9392	0.9346

3.4. Effect of Initial Dye Concentration and Adsorption Isotherms

The influence of initial Congo Red concentration on removal efficiency (R%) using the synthesized Magnetite–LDH–Chitosan nanocomposite is presented in Figure 7A, while the parameters of adsorption isotherm models at 15 and 25 ppm are summarized in Table 2. The nanocomposite exhibited consistently high removal efficiency (99.0–99.9%) over a wide concentration range (3–100 ppm). At lower concentrations (3–10 ppm), the gradual increase in R% indicates the abundance of available active sites. As the dye concentration increased (20–50 ppm), removal efficiency improved due to enhanced mass transfer driving force. At higher concentrations (75–100 ppm), the efficiency stabilized with minor fluctuations, demonstrating the strong adsorption capacity of the material. This performance is attributed to the presence of layered double hydroxide and chitosan, which provide abundant functional groups and interlayer spaces for dye uptake (Asif et al., 2026).

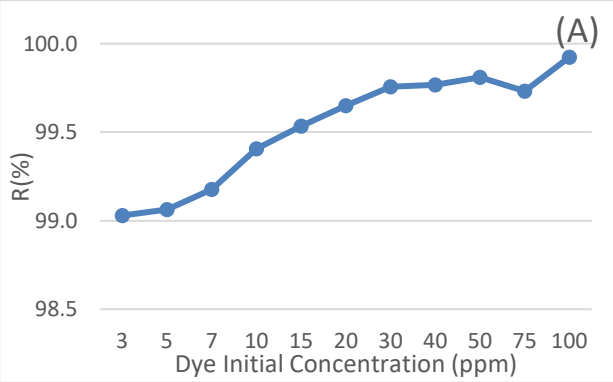

These findings confirm the suitability of the nanocomposite for treating high-strength dye wastewater. The Langmuir isotherm (Figure 7B) showed a good linear fit (R^2 = 0.9024), indicating monolayer adsorption on a homogeneous surface with uniform adsorption sites and minimal interaction between adsorbed molecules.

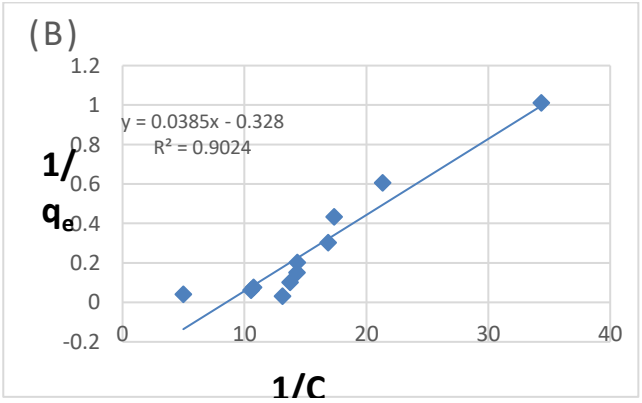

In contrast, the Freundlich isotherm (Figure 7C) exhibited a lower correlation coefficient (R^2 = 0.7014), suggesting poor agreement with heterogeneous multilayer adsorption behavior. This further supports that the adsorption process is predominantly monolayer and homogeneous in nature.

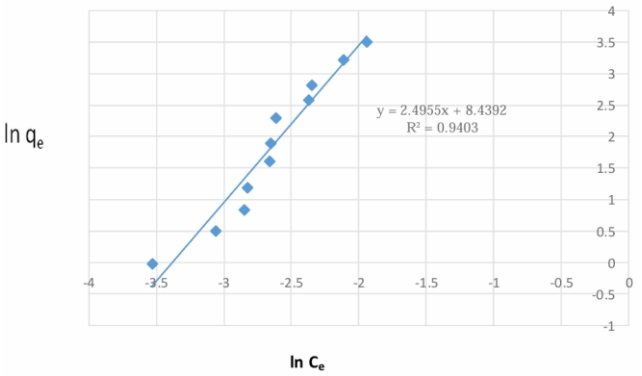

The Dubinin–Radushkevich (D–R) isotherm (Figure 7D) demonstrated a moderate fit (R^2 = 0.7872). The low slope value corresponds to adsorption energy below 8 kJ/mol, indicating that the process is mainly governed by physisorption mechanisms such as electrostatic interactions, pore filling, and surface diffusion.

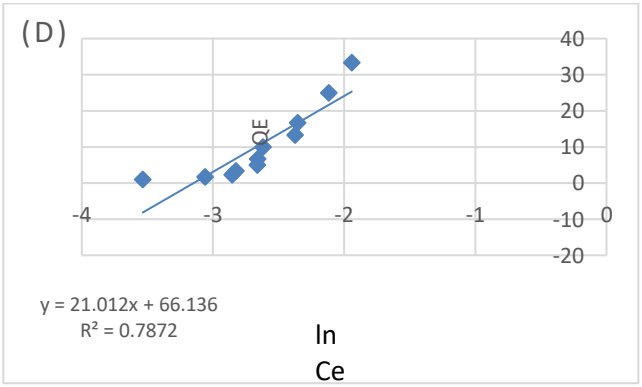

The Temkin isotherm (Figure 7E) showed a relatively strong fit (R^2 = 0.9163), suggesting that adsorption is influenced by adsorbent–adsorbate interactions. The positive slope indicates a gradual decrease in adsorption heat with increasing surface coverage, reflecting the presence of heterogeneous binding sites. Overall, the adsorption of Congo Red onto the Magnetite–LDH–Chitosan nanocomposite is best described by the Langmuir and Temkin models, confirming predominantly monolayer adsorption with contributions from physical interactions. These results highlight the high efficiency and practical applicability of the synthesized nanocomposite for wastewater treatment.

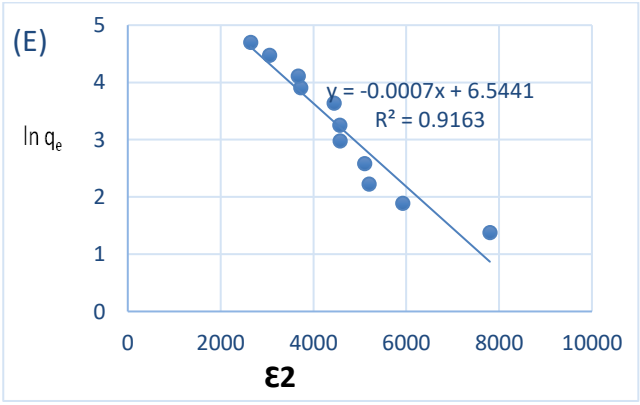

Figure 7: Adsorption isotherms of Congo Red onto Fe_3O_4@Mg/Al-LDH@CS nanocomposite at 25 °C: (A) effect of initial dye concentration on removal efficiency; (B) Langmuir; (C) Freundlich; (D) Dubinin–Radushkevich; (E) Temkin isotherm models.

Table 2. Linear equations and their parameters for different adsorption isotherm models for the 15 ppm and 25 ppm adsorptive removal by the nanocomposite

Isotherm Model	**Linear Equation**	**Linear Plot**	**Isotherm Parameter**	**RRD**
langmuir	$C_e/q_e = 1/q_{max}K_L + C_e/q_{max}$	$1/q_e$ versus $1/C_e$, slope = $1/q_m$, and intercept = $1/(K_L q_{max})$; K_L is the Langmiur constant, q_{max} is the maximum adsorption capacity, $R_L = \frac{1}{1+K_L C_o}$, C_o is the initial concentration of U(IV) ions in mg/L	q_{max} (mg/g)	-3.048333312
			K_L(L/mg)	-8.510635057
			R_L	(-0.04076_-0.00118)
			R^2	0.9024
Freundlich	$\ln(q_e) = \ln(K_F) + 1/n \ln(C_e)$	Ln q_e versus ln C_e, slope = 1/n, and intercept = ln K_F; K_F is the Freunlish constant related to the affinity of the	N	1.42525
			K_F (L/mg)	7.411997714
			R^2	0.7014

		adsorbate to the binding sites of the adsorbent, n is the intensity of the adsorbent		
T e m k i n	$q_e=(RT/b_T)$ ln $(a_T)+(RT/b_T)$ ln (c_e)	q_e versus ln C_e, slope = B = RT/b_T, and intercept = Bln a_T; a_T is Temkin isotherm equilibrium binding constant corresponding to the maximum binding energy, b_T is the Temkin isotherm equilibrium binding constant related to the heat of adsorption and/or the adsorption bonding energy, R is the gas constant = 8.314×10^{-3} kJ mol^{-1} K^{-1}, T is the absolute temperature in K	a_T (L/mg)	23.27861
			b_T(KJ/mol)	0.115933847
			B	21.012
			R^2	0.7872
Dubinin Radushkevich (D–R)	$\ln(q_e)=\ln(q_s)-(K_{ad}\varepsilon^2)$	Ln q_e versus ε^2, slope = K_{ad}, and intercept = Ln (q_s); ε is the *polanyi* potential (ε = RT ln $(1+(1/C_e))$, q_s is the theoretical saturation capacity, K_{ad} is the D-R isotherm constant, $E_s=\frac{1}{\sqrt{2K_{ad}}}$	q_{max} (mg/g)	695.1307796
			K_{ad} (mol^2/J^2)	7.633656584
			E_s(KJ/mol)	0.25599
			R^2	0.9163

3.5. Effect of Adsorbent Dosage and Temperature: Thermodynamic Analysis

The thermodynamic parameters for the adsorption of Congo Red (15 and 25 ppm) onto the magnetite–LDH–chitosan nanocomposite at different temperatures are summarized in Table 3. Figure 8A shows the influence of adsorbent dosage on dye removal efficiency. Increasing the sorbent mass significantly improves removal efficiency due to the greater availability of active adsorption sites. For the 15 ppm solution, a slight fluctuation is observed at low dosages (5–10 mg), likely due to incomplete dispersion or limited interaction. However, efficiency increases sharply beyond 20 mg, reaching a maximum of 99.4% at 40 mg. For the 25 ppm solution, removal efficiency rises rapidly between 5 and 20 mg and stabilizes at approximately 98% at higher dosages, indicating the attainment of adsorption equilibrium. This plateau suggests that most dye molecules are effectively adsorbed, and further increases in dosage do not significantly enhance performance. Overall, the results confirm that adsorption efficiency is dosage-dependent until equilibrium is reached. Figure 8B presents the Van't Hoff plots (ln Kd versus 1/T), which exhibit linear relationships with negative slopes for both concentrations. This behavior indicates that the adsorption process is endothermic. The increase in Kd values with temperature further confirms enhanced adsorption at higher temperatures. The positive values of ΔH° and ΔS°, derived from the slope and intercept, indicate that the process is both endothermic and entropy-driven. The high correlation coefficients (R^2) demonstrate good agreement with the Van't Hoff model. Figure 8C illustrates the effect of temperature (293–328 K) on removal efficiency. For the 15 ppm system, efficiency increases from 96.62% to 99.79%, indicating that adsorption is highly favorable and that the adsorbent surface remains unsaturated. For the 25 ppm system, efficiency also improves slightly with temperature, suggesting enhanced diffusion and interaction between dye molecules and active sites. The positive effect of temperature can be attributed to increased molecular mobility, reduced boundary-layer resistance, improved intraparticle diffusion, and enhanced accessibility of functional groups, particularly due to chitosan swelling. These factors collectively facilitate faster adsorption and improved dye–adsorbent interactions (Hublikar et al., 2026). Thermodynamically, the process follows the Van't Hoff relationship:

$$\Delta G^\circ = \Delta H^\circ - T\Delta S^\circ$$

$$\Delta G^\circ = -RT\ln K_d$$

$$\ln K_d = (\Delta S^\circ)/R - (\Delta H^\circ)/RT, K_d = q_e/C_e$$

Overall, the adsorption of Congo Red onto the magnetite–LDH–chitosan nanocomposite is efficient, temperature-dependent, and governed by endothermic and entropy-driven mechanisms, highlighting its suitability for wastewater treatment applications.

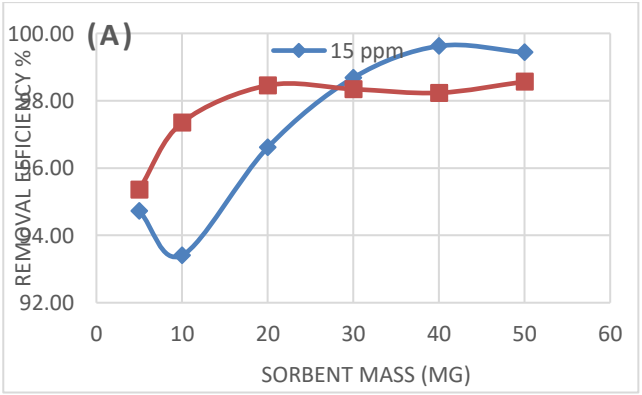

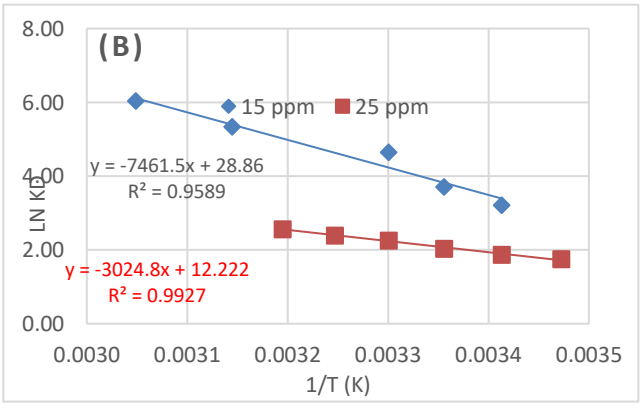

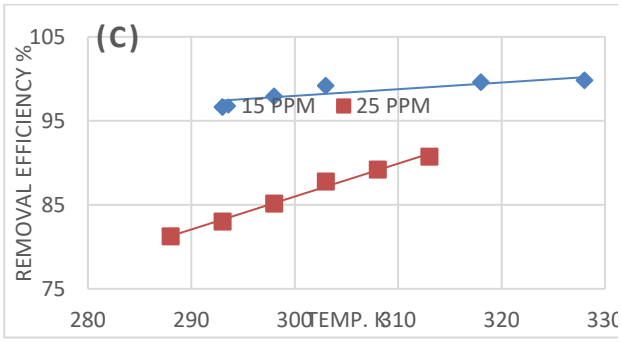

Figure 8: (A) Effect of adsorbent dosage on Congo Red removal efficiency; (B) Van't Hoff plot (ln Kd vs 1/T); (C) effect of temperature (293–328 K) on adsorption performance, indicating an endothermic process.

Table 3. Standard thermodynamic parameters for the adsorption of 15 ppm and 25 ppm onto the Nanocomposite at different reaction temperatures

Dye initial concentration (ppm)	**Temperature (K)**	**LnK$_d$ (L/g)**	**Adsorption Thermodynaic Paramters**			**R^2**
			-ΔG^o (KJmol^{-1})	**ΔH^o (KJmol^{-1})**	**ΔS^o (Jmol^{-1}K^{-1})**	
15 ppm	**293**	2.26	5494.81	-0.23075507	635.27247	0.725
	298	2.73	6763.77			
	308	3.64	9172.66			
	318	4.42	11682.16			
	328	5.11	13945.44			
25 ppm	**293**	2.27	-5526.52	-44.68775	189.93333	0.9927
	298	2.55	-6321.18			
	308	3.72	-9375.41			
	318	4.13	-10918.63			
	328	4.42	-12050.14			

3.6. Regeneration and Reusability of the Magnetite–LDH–Chitosan Nanocomposite

The reusability of the Magnetite–LDH–Chitosan (MLC) nanocomposite was assessed over five consecutive adsorption–desorption cycles using Congo Red as a model dye. After each cycle, the adsorbent was magnetically recovered, washed, dried, and reused. A gradual decrease in adsorbent mass was observed, from 100 mg in the first cycle to 40 mg after the fifth cycle, indicating minor material loss during handling and separation (Figure 9). Despite this reduction, the MLC nanocomposite maintained high removal efficiency, with dye absorbance decreasing from 0.428 to 0.049–0.000 across cycles, corresponding to 88.55–100% removal. The slight decline in performance may be attributed to incomplete desorption, partial blockage of active sites, or minor particle loss (Mavvaji et al., 2026). Overall, the results demonstrate that the MLC nanocomposite exhibits good regeneration capability and structural stability, highlighting its potential for repeated use in sustainable dye removal applications.

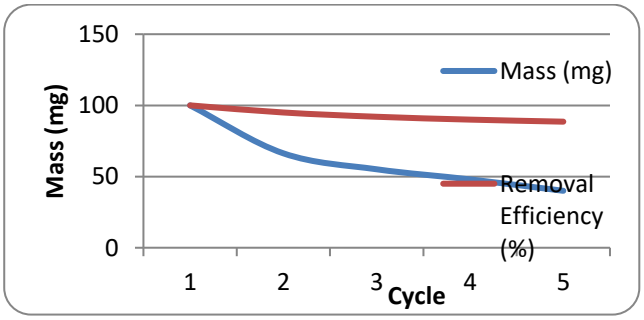

Figure 9: Regeneration and reusability of Fe_3O_4@Mg/Al-LDH@CS nanocomposite over five adsorption–desorption cycles for Congo Red removal.

3.7. Application of MLC for Congo Red Removal from Real Water Samples

The practical performance of the magnetite–LDH–chitosan (MLC) adsorbent was evaluated using three real water matrices, namely tap water (Kobani), industrial wastewater, and seawater (Latakia coast), which differ in ionic strength, turbidity, and organic load. In tap water, MLC exhibited excellent removal efficiency, achieving up to 99.6% at initial dye concentrations of 15 and 25 ppm, indicating strong adsorbent–dye interactions in low-complexity systems (Figure 10). For industrial wastewater, relatively lower efficiencies were observed due to matrix complexity (Yazdizadeh et al., 2025). However, removal improved over successive cycles, reaching 85.09% (15 ppm) and 83.54% (25 ppm), demonstrating good performance in the presence of competing ions and suspended matter.

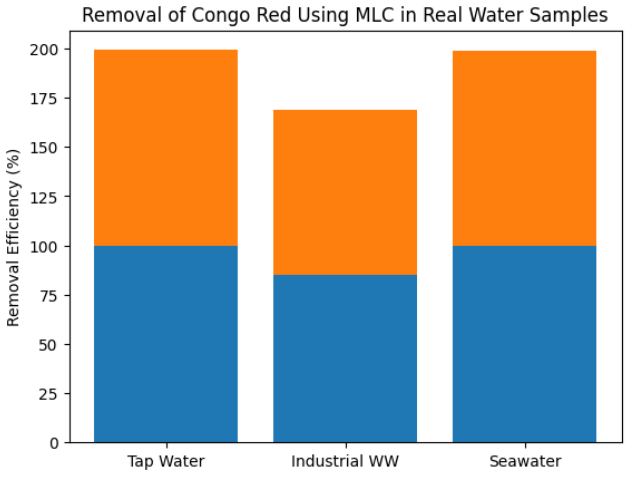

Figure 10: Removal efficiency of Congo Red using Magnetite–LDH–Chitosan (MLC) adsorbent in real water samples (tap water, industrial wastewater, and seawater) at initial dye concentrations of 15 ppm and 25 ppm. The adsorbent shows consistently high performance in low- and high-salinity environments, with slightly reduced efficiency in industrial wastewater due to competing ions and suspended matter.

In seawater, MLC maintained outstanding efficiency (99–100%) across all tested concentrations and cycles, despite high salinity and chloride ion competition, confirming its structural stability and effectiveness under saline conditions. Overall, MLC showed high adsorption efficiency, reusability, and resistance to ionic interference, highlighting its strong potential for practical wastewater treatment applications.

4. Conclusions

This study demonstrates the successful development of a multifunctional Fe_3O_4@LDH@Chitosan nanocomposite for the efficient removal of Congo Red dye from aqueous systems. The integration of magnetite, layered

double hydroxide, and chitosan resulted in a structurally stable material with enhanced adsorption capacity, magnetic separability, and reusability. The microwave-assisted synthesis method provided a rapid and energy-efficient route for producing the composite, aligning with the principles of sustainable material design. Characterization results confirmed the successful formation of the hybrid structure, with strong interactions between its components contributing to improved performance. Adsorption experiments revealed that the nanocomposite achieves high removal efficiencies across a wide range of operating conditions, including variations in pH, temperature, and dye concentration. Kinetic and isotherm analyses indicated that the adsorption process is governed by a combination of chemisorption and physisorption mechanisms, with monolayer adsorption predominating. Thermodynamic evaluation confirmed that the process is spontaneous and endothermic, with improved performance at higher temperatures. The material also demonstrated excellent regeneration capability, maintaining high efficiency over multiple cycles, which is essential for cost-effective wastewater treatment. Importantly, the nanocomposite exhibited strong performance in real water matrices, including seawater and industrial wastewater, highlighting its robustness under complex environmental conditions. This practical applicability distinguishes the material from many laboratory-scale adsorbents that fail under realistic scenarios. Overall, the Fe_3O_4@LDH@Chitosan nanocomposite represents a promising candidate for advanced wastewater treatment applications. Its combination of high efficiency, reusability, and operational simplicity makes it well-suited for scalable implementation in environmental remediation systems. Future work should focus on pilot-scale validation, long-term stability assessment, and evaluation against a broader range of contaminants to further support its practical deployment.

Acknowledgment

The authors would like to express their sincere gratitude to Rojava University and Institute of science and technology for providing access to the laboratory facilities and resources essential for conducting this research.

Authors' contribution

This paper is extracted from a Master thesis, for which Haidar Saify, Mohamed E.Mahmoud and Rehab M .El-Sharkawy were Supervisors of the project, chief investigators, and responsible for the data analysis. Methodology and first draft of the manuscript were done by Jwan Sheikh Mohammad.

Availability of data and material

All required data is in the article, and more details can be request from corresponding author.

Funding

We confirm that this work did not receive any grant from funding agencies in the commercial, public sectors.

Declarations

Conflict of interest

The authors declare that they have no known competing interests.

Reference

1. Arrisujaya, Dian, Yoki Yulizar, and Asep Saefumillah. "Accelerated water purification with magnetite (Iron (II, III) Oxide) nanoparticles: Coagulation applications." J. Chem. Rev 7, no. 1 (2025): 25-62.
2. Asif, Kinza, Muhammad Imran, Anum Shahzadi, Farzana Jamal, Sarmad Frogh Arshad, Anwar Ul-Hamid, Ahmed M. Fouda, and Muhammad Ikram. "Graphene oxide/chitosan-layered double hydroxides for dye decolorization, oxygen evolution reaction and bactericidal inactivation." Materials Science in Semiconductor Processing 201 (2026): 110030.
3. Chaimaa, Amairi, Meriem Bendjelloul, Fatima Zahra Benhachem, El Hadj Elandaloussi, Abdelkader Miraoui, Ahmed Djafri, Ahmed Boucherdoud, Abdelkarim Seghier, and Mohammed Hachemaoui. "Adsorption kinetics and surface interactions of organic dyes and copper ions on a novel biosorbent: raw artichoke hay." Reaction Kinetics, Mechanisms and Catalysis (2026): 1-26.
4. Cui, Lijuan, Xiaokun Shi, Chao Xu, and Shuping Wu. "Recent advances in chitosan-based mixed matrix membranes for efficient wastewater treatment." International Journal of Biological Macromolecules (2026): 150628.
5. Hublikar, Leena V., K. S. Nivedhitha, Bipin S. Chikkatti, Ashok M. Sajjan, Nagaraj R. Banapurmath, D. Palaniswamy, T. Beena, Pradeep Hegde, Sabin Kumar Mishra, and Kartheek Ravulapati. "Functionalized biochar–metal oxide nanocomposites for the catalytic degradation of recalcitrant pollutants in wastewater treatment." RSC advances 16, no. 14 (2026): 12186-12214.
6. Jomardani, Fereshteh, Reza Shakeri, Raziyeh Akbarzadeh, and Syamak Nasiri Kokhdan. "Adsorption kinetics and isotherms of malachite green removal from aqueous solution using TiO2 loaded on f-MWCNTs nanocomposite." Scientific Reports (2026).
7. Kan, Lili, Luohao Lv, Hongran Chen, Bo Wen, Xiangwei Ma, and Fei Wang. "High-temperature resistance of engineered geopolymer composite: Isolating the effects of key components." Construction and Building Materials 481 (2025): 141664.
8. Khan, Rana Rashad Mahmood, Hoorish Qamar, Ayesha Hameed, Aqmar ur Rehman, Muhammad Pervaiz, Zohaib Saeed, Aqib Adnan, and Ayoub Rashid Ch. "Biological and photocatalytic degradation of Congo red, a diazo sulfonated substituted dye: a review." Water, Air, & Soil Pollution 233, no. 11 (2022): 468.
9. Lin, Jiuyang, Wenyuan Ye, Ming Xie, Dong Han Seo, Jianquan Luo, Yinhua Wan, and Bart Van der Bruggen. "Environmental impacts and remediation of dye-containing wastewater." Nature Reviews Earth & Environment 4, no. 11 (2023): 785-803.
10. Mavvaji, Mohammad, Ahmed M. Senan, and Senem Akkoc. "Magnetic layered double hydroxide nanocomposites: synthesis, catalytic performances, environmental and biological applications." Energy & Environmental Materials 8, no. 5 (2025): e70015.
11. Mystrioti, Christiana, Nymphodora Papassiopi, and Anthimos Xenidis. "Synthesis of Iron Nanomaterials for Environmental Applications from Hydrometallurgical Liquors." Minerals 12, no. 5 (2022): 556.
12. Oguanobi, Nonso C., Chukwunonso O. Aniagor, George Okoronkwo, Calistus N. Ude, Chijioke E. Onu, and Ephrem N. Anike. "Industrial dye effluent sources, generation, and value-added products." In Engineered Biocomposites for Dye Adsorption, pp. 1-10. Elsevier, 2025.
13. Tundwal, Aarti, Harish Kumar, Priti Yadav, Varsha Yadav, and Bindu Mangla. "Chitosan, conducting polymer, and metal oxide nanocomposites: Mechanistic insights and sustainable approaches for water treatment." Next Materials 10 (2026): 101559.
14. Wang, Kun, Chaoqun Zhu, Yinghua Li, Xin Guo, Mingchuan Zhang, and Xi Chen. "Approaches for effective layered double hydroxides for advanced oxidative degradation of emerging pollutants

harnessing natural solar light." Chemical Engineering Research and Design (2026).

15. Xiao, Wuyang, Fuhe Le, Rui Sheng, Xue Yang, Xueying Cao, and Wei Jia. "Constructing Dual Active Sites via Cu Doping in Perovskite for Boosting Electrochemical Hydrogen Evolution." ChemCatChem 18, no. 3 (2026): e01581.
16. Yazdizadeh, Shirin, S. Yousef Ebrahimipour, S. Jamilaldin Fatemi, Moj Khaleghi, and Samaneh Ramezanpour. "Mesoporous Fe3O4@ SiO2@ La nanocomposite for efficient methylene blue removal from wastewater." Journal of Molecular Structure 1322 (2025): 140337.
17. Younas, Fazila, Adnan Mustafa, Zia Ur Rahman Farooqi, Xiukang Wang, Sadia Younas, Waqas Mohy-Ud-Din, Muhammad Ashir Hameed et al. "Current and emerging adsorbent technologies for wastewater treatment: Trends, limitations, and environmental implications." Water 13, no. 2 (2021): 215.
18. Zazouli, Mohammad Ali, Zabihollah Yousefi, Esmaeil Babanezhad, and Alireza Ala. "Evaluation of combined efficiency of conventional coagulation-flocculation process with advanced oxidation process (sulfate-hydroxyl radical) in leachate treatment." Environmental Engineering Research 29, no. 3 (2024).
19. Zhang, Zekai, Xiaoyu Liu, Jinping Zhao, Jin Zhou, Zhuang Liu, and Liang-Yin Chu. "Layered double hydroxide separation membranes: advances and prospects in water purification applications." Green Chemical Engineering (2026).